Explanation for the 4.8-V plateau in $LiCr_xMn_{2-x}O_4$

M. N. Obrovac
Department of Physics, Dalhousie University, Halifax, Nova Scotia, Canada B3H 3J5

Yuan Gao
FMC Corporation, Highway 161, Gastonia, North Carolina 28054-0020

J. R. Dahn*
Departments of Physics and Chemistry, Dalhousie University, Halifax, Nova Scotia, Canada B3H 3J5

(Received 15 August 1997; revised manuscript received 19 November 1997)

Using the results of photoelectron spectroscopy (PES) measurements on $LiCr_xMn_{2-x}O_4$ we provide an explanation for the origin of the 4.8-V plateau in $Li/LiCr_xMn_{2-x}O_4$ cells. PES shows that the d bands derived from Mn $3d$ e_g are about 0.5 eV more weakly bound than the d bands derived from Cr $3d$ t_{2g}. Within a rigid-band formalism, as lithium atoms are removed from $LiCr_xMn_{2-x}O_4$, the electrons are first removed from Mn e_g. When these electrons are gone, the next electrons available are those in Cr t_{2g}, which are bound more tightly by 0.5 eV. Thus, at this point, the voltage of a $Li/LiCr_xMn_{2-x}O_4$ cell steps up from 4.1 to 4.8 V. The oxidation states on the atoms in the compound are $Li^{+1}Cr_x^{+3}Mn_{2-x}^{+3}Mn^{+4}O_4^{-2}$ so the step in voltage should occur when the $(1-x)$ Mn^{3+} atoms are all oxidized to Mn^{4+}, or when $(1-x)$ Li have been removed from the compound. Using a series of carefully prepared and characterized samples, we show that this is true for single phase samples that do not exhibit cation mixing. [S0163-1829(98)02310-8]

INTRODUCTION

Currently most commercially available lithium ion batteries use $LiCoO_2$ as a cathode material. Because of its environmental and economical advantages, $LiMn_2O_4$ is an attractive alternative to $LiCoO_2$. In an effort to improve cycling behavior, other transition metals have been substituted for manganese to make $LiCr_xMn_{2-x}O_4$ M=Ti, V, Cr, Fe, Co, Ni, Cu, Zn, etc.).[1,2] Often these substitutions cause significant changes in the voltage profile that are hard to understand. If there is no significant cation mixing, the immediate environment around the lithium ion should be relatively unchanged by these substitutions. Thus the chemical potential of the lithium ion should also not be significantly different from stoichiometric $LiMn_2O_4$. It is most likely, then, that the changes in the voltage profiles by these substitutions arise because of changes in the electronic structure.

In another paper of ours we studied the change in voltage profiles of $LiNi_xMn_{2-x}O_4$ with changes in the valence band measured by ultraviolet photoelectron spectroscopy (UPS), as a function of the nickel content, x.[3] Using a rigid-band model, which is described elsewhere,[4] we showed that the high-voltage plateau at 4.7 V in $Li/LiNi_xMn_{2-x}O_4$ cells is due to the increased energy required to remove electrons from the Ni $3d$ levels compared to the Mn $3d$ e_g levels. Recently, Sigala and co-workers[6] have observed a 4.8-V plateau in $Li/LiCr_xMn_{2-x}O_4$ cells. They found that the capacity of the 4.8-V plateau increased linearly as x increases at the expense of the 4.1-V plateau. In this paper we study the valence band of $LiCr_xMn_{2-x}O_4$ using synchrotron radiation photoelectron spectroscopy (PES) as a function of x. We propose a similar model to describe the voltage behavior of these materials as we proposed for the nickel substituted spinels.

EXPERIMENT

$LiCr_xMn_{2-x}O_4$ $(0.17 \leqslant x \leqslant 0.83)$ materials were prepared by the sol-gel method. Stoichiometric amounts of $CrNO_3 9H_2O$ (Aldrich), $LiNO_3$ (Aldrich), and $Mn(CH_3COO)_2 4H_2O$ (Sigma) were dissolved in a minimum amount of distilled water. Concentrated ammonium hydroxide (Fisher) was added dropwise to the stirring solution until the pH was 9. The solution was allowed to stir for 1 h. During this time the solution became viscous due to the formation of a blue gel. The gels were partially dried overnight at 90 °C and then heated in air at 300 °C for 24 h and reground. A series of $LiCr_xMn_{2-x}O_4$ samples heated to different final temperatures was prepared by reheating at 500 °C, 600 °C, or 700 °C in air for 18 h. The samples were then cooled at 50 °C/h to room temperature.

Powder x-ray-diffraction measurements were made with a Siemens D5000 powder diffractometer equipped with a copper target x-ray tube and a diffracted-beam monochromator. All specimens were measured from 10° to 80° in scattering angle and each data collection took approximately 2 h. For samples with $x > 0.66$ prepared at temperatures less than 600 °C, peaks corresponding to a metastable cubic phase of a chromium oxide[5] were observed. No impurity peaks were detected in the other samples.

The x-ray data was analyzed using Hill and Howard's version[7] of the Rietveld program. In the refinements, the samples were assumed to have the spinel structure. Only manganese was assumed to occupy the 16d sites. When the cubic chromium oxide phase was present, both phases were included in the refinement. For all the refinements, the goodness of fit (χ^2) and the Bragg R factor (R_B) were better than 6% and 4% respectively. The results of these refinements are listed in Table I.

TABLE I. Lattice constants of $LiCr_xMn_{2-x}O_4$ samples calculated by the Rietveld refinement method.

Temp. (°C)	x	a (Å)	GOF	R_B
	0.17	8.194	1.26	1.93
	0.33	8.185	2.86	1.74
300 °C	0.50	8.176	2.01	1.99
	0.67	8.173	2.29	2.91
	0.83	8.174	2.71	3.18
	0.17	8.217	1.31	0.94
	0.33	8.209	2.68	0.65
500 °C	0.50	8.193	1.30	0.98
	0.67	8.185	1.68	1.57
	0.83	8.189	1.85	2.59
	0.17	8.225	3.28	2.26
	0.33	8.216	2.93	2.41
600 °C	0.50	8.204	1.39	1.84
	0.67	8.196	1.29	1.36
	0.83	8.196	1.40	1.89
	0.17	8.236	5.34	3.67
	0.33	8.223	5.27	3.57
700 °C	0.50	8.212	1.26	0.98
	0.67	8.200	5.15	3.84
	0.83	8.198	1.36	1.67

More careful 12 h x-ray-diffraction measurements from 10° to 120° were done on the samples prepared at 500 °C and on those samples with $x=0.5$. In the Rietveld refinements of this data, both chromium and manganese were assumed to occupy the 16*d* sites, but the chromium to manganese ratio was fixed to the sample stoichiometry. For these refinements, χ^2 and R_B were better than 2% and 4%, respectively. The results of the refinements are given in Table II. Because of the presence of the cubic chromium oxide phase in the 500 °C sample, meaningful occupation numbers for this sample could not be obtained.

The electrochemical behavior of the cathodes was evaluated in 2320 coin-type cell hardware. Details of the cell hardware have been described elsewhere.[8] The cell stack consisted of a $LiCr_xMn_{2-x}O_4$ composite cathode, a Celgard 2502 microporous polypropylene separator soaked with an electrolyte of 1 M $LiPF_6$ in a 30/70 volume mixture of ethylene carbonate and diethyl carbonate, and a lithium metal foil anode.

TABLE II. Occupation numbers of 500 °C samples and samples with $x=0.5$ calculated by the Rietveld refinement method.

Temperature	x	X_{8a}[a]	X_{16d}[a]	χ^2	R_B
500 °C	0.17	0.291	0.495	1.86	1.55
500 °C	0.33	0.299	0.493	2.01	1.60
500 °C	0.50	0.329	0.482	2.02	3.61
500 °C	0.67	0.302	0.476	1.69	1.68
300 °C	0.5	0.389	0.454	1.98	1.69
500 °C	0.5	0.329	0.482	2.02	3.61
600 °C	0.5	0.295	0.495	1.60	3.56
700 °C	0.5	0.258	0.499	2.11	2.02

[a]Occupation numbers are given as fractions of the oxygen occupation number.

$LiCr_xMn_{2-x}O_4$ composite cathodes were prepared by a method developed by the Bellcore Corporation.[9] A slurry was prepared of 11.1% $LiCr_xMn_{2-x}O_4$ powder, 1.4% Super *S* carbon black (Chemetals Inc.), 5.6% polyvinylidene difluoride (PVDF)/hexafluoropropylene (88/12 by weight) binder (Kynar Flex 2801), 9.7% of a 50/50 volume solution of ethylene carbonate (EC)/propylene carbonate (PC) (added as a plasticizing agent), and 72.2% acetone by weight. The slurry was mixed for 4 h at 60 °C, until the PVDF binder was dissolved, and then was immediately spread by means of a doctor blade with a 0.025″ gap onto a glass plate. After the acetone evaporated, the cathodes were cut into 1.2 cm-diameter disks with a punch. Before use in cells, the cathodes were placed in anhydrous diethyl ether for 5 min to extract the EC/PC plasticizer. The resulting cathodes were planned to consist of 61.3% active material, 7.7% carbon black, and 30.9% PVDF binder by weight.

Prior to cell assembly, the cathodes were weighed before the EC/PC had been extracted and it was assumed incorrectly that no EC/PC loss had occurred during storage in tightly sealed bags. After the study, it was found that during cathode storage, significant amounts of the EC/PC plasticizer had evaporated during storage. Thus, the calculated active weights of the cathodes were probably too low.

The cells were cycled under thermostatic conditions at 30 °C between 2 V and 5.3 V using constant current cyclers with $\pm 1\%$ current stability. *C* rate is defined here as the current required to remove one equivalent of lithium from the $LiCr_xMn_{2-x}O_4$ sample in 1 h. This would correspond to a current of 148.0 mAh/g for stoichiometric $LiMn_2O_4$. Cells were charged at *C*/10 rate and discharged at *C*/20 rate. The high charging rate was used in an attempt to minimize side reactions with the electrolyte at high voltages.

PES studies were carried out at the Canadian Grasshopper beamline located at the Synchrotron Radiation Center of the University of Wisconsin at Madison. The synchrotron beam was monochromatized by a Mark IV Grasshopper grazing incidence monochromator with an energy range of 50–800 eV. The dispersion of the monochromator with the smallest slit setting is 0.03 Å. The photoelectrons were detected with a Leybold 180° hemispherical electron energy analyzer. It has a resolution of 0.8 eV with 100 eV pass energy. Details of the beamline can be found elsewhere.[10]

PES samples were prepared by thoroughly mixing an approximately 50/50 volume mixture of the sample powder and Super *S* Carbon Black (Chemetals Inc.) to avoid sample charging. We have previously used carbon black to eliminate sample charging in PES measurements of nonconducting powders. A study of the method can be found in Ref. 11. The powder samples were mounted with copper electrical tape onto a stainless-steel block, which was grounded throughout the measurement. Measurements were carried out under ultrahigh vacuum conditions with the measurement chamber typically at $2-4\times10^{-9}$ Torr. All measurements were made with an incident photon energy of 130 eV.

RESULTS AND DISCUSSION

Rietveld refinement results

Table I lists the lattice constants of the $LiCr_xMn_{2-x}O_4$ samples as a function of x. The lattice constant decreases and then reaches a limiting value with increasing chromium content. This may be due to the slightly smaller ionic radius of Cr^{3+} (0.63 Å), compared to Mn^{3+} (0.66 Å). As the preparation temperature is increased, the lattice constant also increases. If oxygen was lost by the samples during heating, the oxidation number of the cations would decrease and their ionic radius would increase, which may cause in increase in the lattice constant. However, thermogravimetric analysis did not reveal any oxygen loss in the samples below 700 °C.

The dependence of the occupation numbers on the chromium content and on the preparation temperatures from more careful Rietveld measurements are listed in Table II. While the 16*d* occupation number is very nearly its theoretical value of 0.5 for all the samples, the 8*a* occupation number is always higher than its theoretical value and does not vary much with the chromium content. If chromium or manganese were to occupy some of the lithium sites, this would cause the Rietveld program to increase the occupation number of the 8*a* sites to compensate for the significantly larger scattering power of chromium and manganese compared to lithium. Thus, the high occupation numbers in the 8*a* sites might indicate cation mixing.

Table II shows that the 8*a* occupation number in the 500 °C samples does not change significantly as the chromium content increases. However there is a definite increase in the 8*a* occupation number as the preparation temperature is decreased. This means the extent of cation mixing is more strongly affected by the preparation temperature than on the chromium content. This makes sense, since according to ligand field theory, Cr^{3+}, Mn^{3+}, and Mn^{4+} are more stable in octahedral sites than in tetrahedral sites. Thus, increasing the chromium content ought not have much effect on cation mixing in the 8*a* sites.

Electrochemical results

In general, the discharge capacity between 5.3 and 3.0 V of the $LiCr_xMn_{2-x}O_4$ materials varied by about 30% from sample to sample and did not show any general trends with respect to the chromium content or preparation temperatures. This may have been caused by plasticizer evaporation prior to cathode weighing, the charge used up in electrolyte decomposition reactions above 4.5 V or because of the unknown amount of the cubic chromium oxide phase present in the samples prepared below 600 °C and having $x>0.5$.

Figure 1 shows the discharge curves between 3.5 and 5.0 V of the samples prepared at 600 °C. To make direct comparisons, the curves have been normalized so that their capacity at 3.35 V is 150 mAh/g. Excepting the sample with $x=0.83$, the voltage curves have a high-voltage plateau at about 4.8 V that increases in capacity at the expense of the 4.1-V plateau as the chromium content is increased. As previously mentioned, this observation was earlier reported by Sigala *et al.*[6] The sample with $x=0.83$ has almost no capacity above 4.5 V and is almost featureless. This sample showed significant electrolyte reactions during charging and probably never reached its fully charged state. In addition, Sigala *et al.* observed poor cyclability for samples with $x \geqslant 0.75$ that may indicate structural changes occur for materials with high chromium contents during cycling.[6]

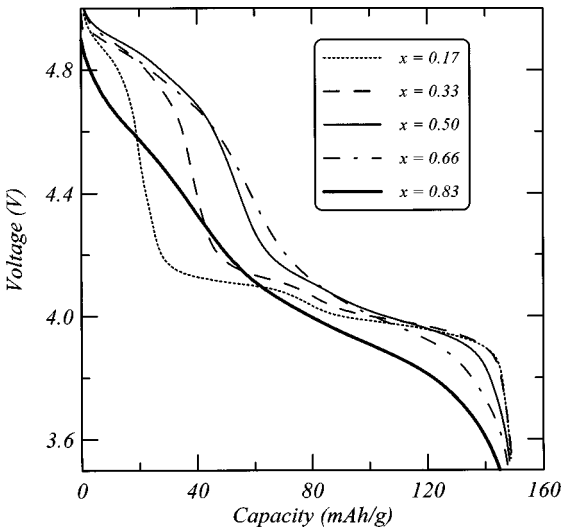

FIG. 1. The discharge curves of $LiCr_xMn_{2-x}O_4$ ($0.17 \leqslant x \leqslant 0.83$) prepared at 600 °C.

Samples prepared at 700 °C produced voltage curves similar to that of the 600 °C samples. Samples prepared at temperatures below 600 °C had very little capacity above 4.5 V. This may be due to the larger extent of cation mixing observed for the low-temperature samples.

To explain the almost 1:1 increase in the 4.8-V plateau capacity with x observed in the 600 °C and 700 °C samples, a model, similar to that used to explain the high-voltage behavior of nickel substituted spinels,[3] is used to describe this behavior.

For $LiMn_2O_4$ spinel, the half reaction at the cathode during charging for the 4.1-V plateau may be written as

$$Li^+Mn^{3+}Mn^{4+}O_4 \rightarrow Mn_2^{4+}O_4 + Li^+ + e^-. \quad (1)$$

Thus the capacity of the 4.1-V plateau is due to the oxidation of Mn^{3+} to Mn^{4+}. The 1:1 decrease in the capacity of the 4.1-V plateau as the chromium content is increased could be explained if we assumed the addition of chromium replaces the Mn^{3+} with Cr^{3+}, making $Li^+Cr_x^{3+}Mn_{1-x}^{3+}Mn^{4+}O_4$. Then the capacity of the 4.1-V plateau due to the oxidation of Mn^{3+} would be decreased by a factor of $(1-x)$:

$$Li^+Cr_x^{3+}Mn_{1-x}^{3+}Mn^{4+}O_4 \rightarrow Li_x^+Cr_x^{3+}Mn_{2-x}^{4+}O_4 + (1-x)Li^+ + (1-x)e^-. \quad (2)$$

Further charging might proceed by the oxidation of Cr^{3+} to Cr^{4+}, this would mean a second voltage plateau due to the reaction

$$Li^+Cr_x^{3+}Mn_{2-x}^{4+}O_4 \rightarrow Cr_x^{4+}Mn_{2-x}^{4+}O_4 + xLi^+ + xe^-. \quad (3)$$

This reaction increases in capacity in a 1:1 ratio as x is increased, as is observed for the 4.8-V plateau capacity.

In order to verify this model, a parameter, η, was defined as the fraction of the 4.8-V plateau capacity to the total of the 4.8-V and the 4.1-V plateau capacities. The 4.8-V plateau

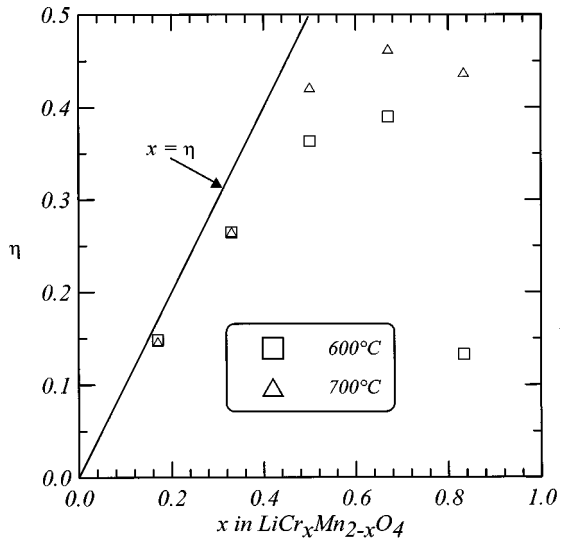

FIG. 2. The fraction of the 4.9-V plateau capacity to the total 4.1 V and 4.8 V capacities (η) plotted as a function of the chromium content in $LiCr_xMn_{2-x}O_4$ samples prepared at 600 °C and 700 °C.

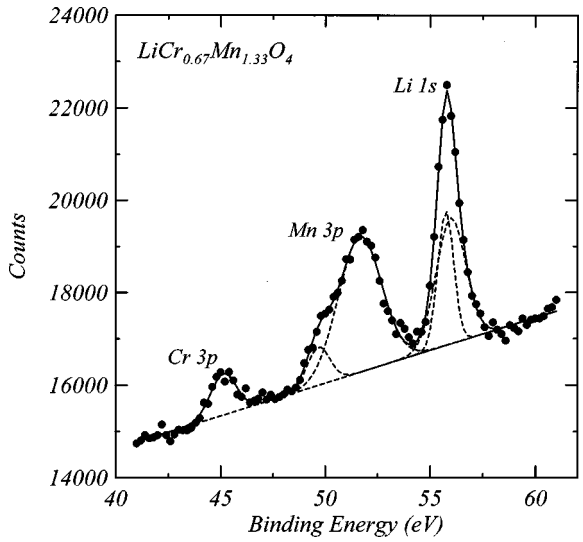

FIG. 3. Core-level spectrum of $LiCr_{0.67}Mn_{1.33}O_4$ Gaussian fits to the individual peaks in the spectrum are indicated by the dashed lines. The solid line represents the sum of the Gaussian fits.

capacity was taken to be between 4.4 V to 4.3 V and the total 4.8-V and 4.1-V plateau capacity was taken to be between 3.35 V and 5.3 V. According to Eqs. (2) and (3), the dependence of η on x should be $\eta = x$. A plot of η vs the chromium content is shown in Fig. 2. Although the $x = 0.2$ sample lies close to the theoretical line, the experimental points diverge on the low η side of the line as the chromium content is increased. Because of current losses during discharge above 4.5 V due to electrolyte decomposition, the observed capacities of the 4.8-V plateau are probably lower than their actual values. Thus low values of η are to be expected. Furthermore, as the chromium content is increased and the 4.8-V plateau capacity is correspondingly increased, more charge is being lost in electrolyte decomposition and the value of η would become progressively lower. The $x = 0.83$ sample is an extreme case since for this sample the electrolyte decomposition was so severe that the sample probably never reached a fully charged state.

Although Eqs. (2) and (3) seem to correctly describe the behavior of the 4.8-V plateau if electrolyte decomposition reactions are taken into account, they give no information as to why the oxidation of Cr^{3+} should occur at a higher voltage than that of Mn^{3+}. To explain this a model of the electronic structure of $LiCr_xMn_{2-x}O_4$ was developed using the results of PES measurements.

Results of PES core-level measurements

Core-level spectra of $LiCr_xMn_{2-x}O_4$ powders were measured between 41 and 61 eV. Figure 3 shows a typical core-level spectrum. The three main peaks in the spectrum were assigned to the Cr $3p$, Mn $3p$, and the Li $1s$ core levels, respectively. Gaussian fits were made to the peaks to find their integrated intensities. The Mn $3p$ and Li $1s$ peaks appear to be comprised of more than one component, so two Gaussians were used to fit each of them. From the integrated intensities, it became clear that the surface of the materials did not have the same composition as the bulk. Because neither the thickness nor the electron escape depth of the surface layer was known, only qualitative observations were made on the surface composition, based on the integrated intensities corrected for the photionization cross section[12] alone.

Figures 4(a)–4(c) show the fraction of the total peak area of the Mn $3p$, Li $1s$, and Cr $3p$ peaks, respectively, as a function of the chromium concentration. In all the samples, the amount of chromium on the surface increases with x, except for the samples prepared at 300 °C in which the chromium content remains approximately constant. The lithium content also increases on the surface with increasing x for all the samples, despite the fact that the lithium content is presumably the same in all the bulk materials. As predicted from stoichiometry, the manganese content decreases linearly with x. However, the manganese content on the surface increases while the lithium content decreases at all values of x with increasing temperature.

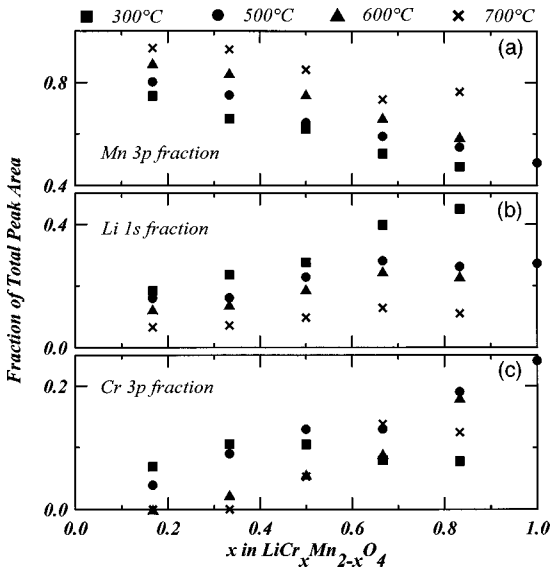

FIG. 4. The fraction of the total core-level peak area contained in the (a) Mn $3p$, (b) Li $1s$, and (c) Cr $3p$ peaks.

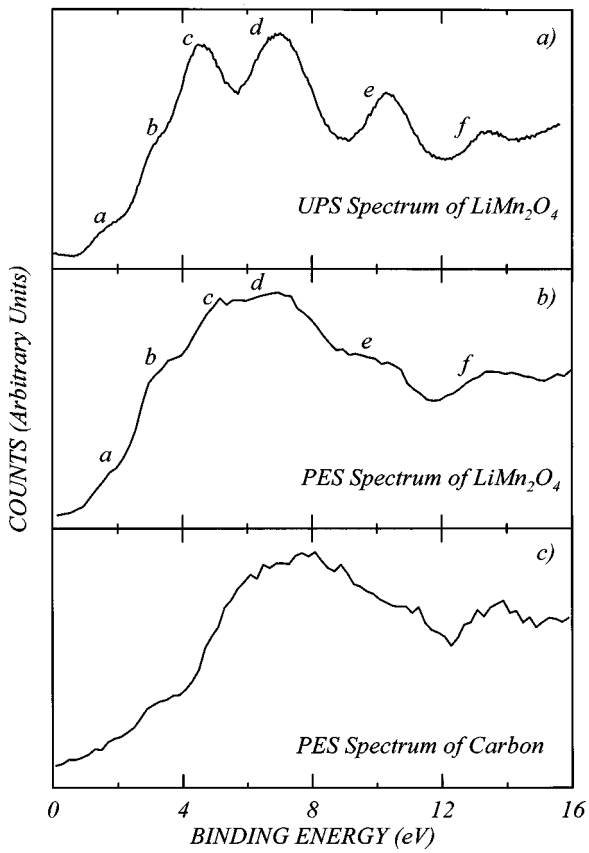

FIG. 5. (a) The UPS spectrum of $LiMr_2O_4$ from a previous study of ours. ($h\nu = 40.8$ eV), (b) The PES spectrum of the same sample of $LiMn_2O_4$ mixed with carbon black. ($h\nu = 130$ eV). (c) The PES spectrum of carbon black. ($h\nu = 130$ eV). Binding energies are measured with respect to the carbon black valence band.

Based on these results, a manganese compound, most probably an oxide of manganese, is the most thermodynamically favored species on the surface, while lithium and chromium are less favored on the surface. It is not clear why the lithium content on the surface increases with x, unless lithium is also more favored on the surface than chromium. Some theoretical modeling of this effect could be the subject of future work.

Results of PES valence-band measurements

Figure 5(a) shows the UPS valence band spectrum of a $LiMn_2O_4$ sample without carbon black from a previous study of ours.[3] We identified the features in the UPS spectrum by comparing with the extensively studied valence bands of manganese monoxide that has a high spin configuration. In both oxides the manganese atoms are octahedrally coordinated to oxygen atoms. Features a and b were attributed to the Mn $3d$ e_g and t_{2g} levels, respectively. Features c and d were attributed to the oxygen $2p$ orbitals. Feature e was identified as the so-called satellite peak, the origin of which has been the subject of debate for years. We are unclear about the origin of feature f.

Figure 5(b) shows the PES spectrum of the same sample of $LiMn_2O_4$ mixed with carbon black. Most of the features of the UPS spectrum are clearly visible in the PES spectrum. However, features b, d, e, and f are nearly coincidental with similar features in the valence-band spectrum of carbon black in Fig. 5(c). It is difficult to tell what relative contributions carbon black and $LiMn_2O_4$ make to these features. There are no features in the carbon black valence band near feature a, the Mn $3d$ e_g level.

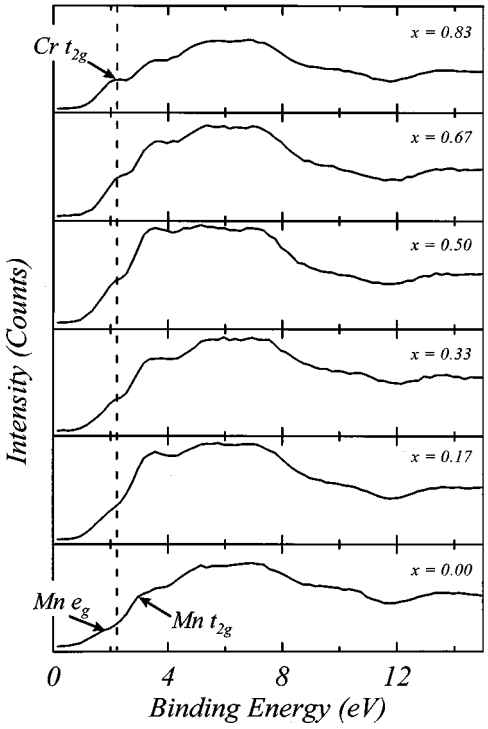

FIG. 6. The valence-band spectra of $LiCr_xMn_{2-x}O_4$ ($0.17 \leqslant x \leqslant 0.83$) prepared at 600 °C Binding energies are measured with respect to the valence band of carbon black.

Figure 6 shows the PES valence-band spectra of $LiCr_xMn_{2-x}O_4$ samples prepared at 600 °C. A new feature in the valence band at about 2.2 eV that grows larger with increasing chromium content can clearly be seen in the spectra. This feature is about 0.5 eV higher in binding energy than the Mn $3d$ e_g and was assigned to the Cr $3d$ t_{2g} level, which is the highest occupied level in Cr^{3+}, even though the level may have some Mn $3d$ character. Similar results were observed in the valence spectra of the 500 °C samples. However, the 2.2 eV peak was very weak in the samples prepared at 300 °C where, according to Fig. 4, the chromium concentration remains small on the surface, even for large x. The valence band of the 700 °C samples with $x > 0.5$ was not measured. In all the samples the Mn $3d$ e_g was hard to see. This may be because, according to Fig. 4, the manganese content on the surface decreases as the chromium content is increased.

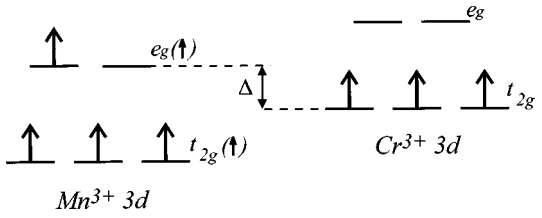

FIG. 7. The alignment of the Mn^{3+} $3d$ levels to the Cr^{3+} $3d$ levels in $LiCr_xMn_{2-x}O_4$. The energy difference between the Mn e_g level and the Cr t_{2g} level is defined as Δ and is about 0.5 eV.

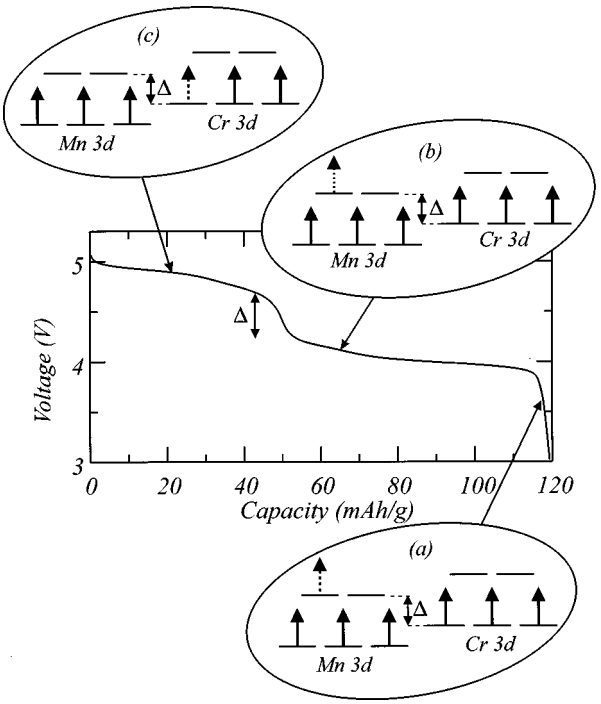

FIG. 8. The change in the occupation of the valence-band levels in $LiCr_{0.5}Mn_{1.5}O_4$ during the charging process. Partially empty levels are shown with dashed lines.

With the knowledge of the position of the Cr $3d$ t_{2g} level in relation to the Mn $3d$ e_g level, a simple picture of the valence bands, shown in Fig. 7, was made. The Cr $3d$ t_{2g} level lies between the Mn $3d$ t_{2g} and the Mn $3d$ e_g levels and is about 0.5 V higher in binding energy than the Mn $3d$ e_g level. The position of the Cr $3d$ e_g level is not known, but is believed to be above the Fermi level and is shown in Fig. 7 for completeness.

Using Fig. 7, the origin of the 4.8-V plateau, which was thought to coincide with the oxidation of Cr^{3+}, can now be explained. During charge, the lithium deintercalates from the $LiCr_xMn_{2-x}O_4$ cathode material. According to the rigid-band model, this will cause the valence d orbitals in the cathode to rise in energy, but electrons removed from the cathode would correspondingly lower the Fermi level, keeping the voltage approximately constant. Initially during charge, the electrons removed from the cathode would be the least bound Mn $3d$ e_g electrons. However, as charging proceeds, these electrons are exhausted and electrons from the next least bound level must be removed. According to Fig. 7 these are the Cr $3d$ t_{2g} electrons, which are about 0.5 eV higher in binding energy than the Mn $3d$ e_g electrons. The extra energy required to remove the electrons requires that the voltage must be increased for charging to proceed, thus a new high-voltage plateau is observed on the voltage curve. Figure 8 summarizes the model by indicating which levels are filled, empty, or partially filled (dashed arrows) during the charging process.

CONCLUSIONS

PES measurements have shown that the reason for the step between the 4.1-V and 4.8-V plateaus in $Li/Li_yCr_xMn_{2-x}O_4$ cells is the 0.5 eV offset between the Mn $3d$ e_g and the Cr $3d$ t_{2g} levels in $Li_yCr_xMn_{2-x}O_4$. Apparently, the Li^+ ion chemical potential does not vary strongly with x at fixed y, so that the step in voltage is caused by the sharp change in the electron chemical potential that occurs when the amount of lithium removed per formula unit is equal to $(1-x)$, or when all the Mn^{3+} ions have been oxidized to Mn^{4+}. On the other hand, the small step in voltage that occurs near 80 mAh/g ($y=\frac{1}{2}$) in Fig. 1 is apparently caused by the filling of an ordered arrangement of Li^+ ions,[13] due to repulsive interactions between the Li^+ ions. This small step is thus caused by variations in the Li^+ chemical potential with Li composition, y. Therefore, $LiCr_xMn_{2-x}O_4$ is an excellent material for pedagogical purposes, for it shows the importance of both the ionic and electronic contributions to the chemical potential of the intercalated Li atom. It is our belief that electron spectroscopy measurements can provide similar insights into many other electrode materials.

*Author to whom correspondence should be addressed.

[1] J. M. Tarascon, E. Wang, F. K. Shokoohi, W. R. McKinnon, and S. Colson, J. Electrochem. Soc. **138**, 2859 (1991).
[2] R. J. Gummow, A. de Kock, and M. M. Thackeray, Solid State Ionics **69**, 59 (1994).
[3] Yuan Gao, K. Myrtle, and J. R. Dahn, Phys. Rev. B **54**, 16 670 (1996).
[4] W. R. McKinnon, in *Solid State Electrochemistry*, edited by Peter G. Bruce (Cambridge University Press, Cambridge, England, 1995), p. 163.
[5] A. W. Laubengayer and H. W. McCune, J. Am. Chem. Soc. **74**, 2362 (1952).
[6] C. Sigala, D. Guyomard, A. Verbaere, Y. Piffard, and M. Tournoux, Solid State Ionics **81**, 167 (1995).
[7] R. J. Hill and C. J. Howard, J. Appl. Crystallogr. **18**, 173 (1985).
[8] A. M. Wilson and J. R. Dahn, J. Electrochem. Soc. **142**, 326 (1995).
[9] Antoni Godz, Caroline Schmutz, Jean-Marie Tarascon, and Paul Warren, International Patent No. PCT/US 94/08772 (2 August 1994).
[10] K. H. Tan, G. M. Bancroft, L. L. Coatsworth, and B. W. Yates, Can. J. Phys. **60**, 131 (1982).
[11] M. N. Obrovac, Yuan Gao, M. N. Richard, and J. R. Dahn, Appl. Phys. Lett. **71**, 2262 (1997).
[12] J. J. Yeh and I. Lindau, At. Data Nucl. Data Tables **32**, 1 (1985).
[13] Yuan Gao, J. N. Reimers, and J. R. Dahn, Phys. Rev. B **54**, 3878 (1996).